Published in final edited form as:
Biochemistry. 2010 December 14; 49(49): 10565–10573. doi:10.1021/bi101480z.

The Efavirenz Binding Site in HIV-1 Reverse Transcriptase Monomers†

Valerie A. Braz[‡], **Mary D. Barkley**[‡,§,*], **Rebecca A. Jockusch**[||], and **Patrick L. Wintrode**[§,*]

[‡] Department of Chemistry, Case Western Reserve University, 10900 Euclid Avenue, Cleveland, Ohio 44106

[§] Department of Physiology and Biophysics, Case Western Reserve University, 10900 Euclid Avenue, Cleveland, Ohio 44106

[||] Department of Chemistry, University of Toronto, Toronto, Ontario, Canada M5S 3H6

Abstract

Efavirenz (EFV) is a potent nonnucleoside reverse transcriptase inhibitor (NNRTI) used in the treatment of AIDS. NNRTIs bind in a hydrophobic pocket located in the p66 subunit of reverse transcriptase (RT), which is not present in crystal structures of RT without inhibitor. Recent studies showed that monomeric forms of the p66 and p51 subunits bind efavirenz with micromolar affinity. The effect of efavirenz on the solution conformations of p66 and p51 monomers was studied by hydrogen/deuterium exchange mass spectrometry (HXMS) and Fourier transform ion cyclotron resonance mass spectrometry (FT-ICR MS). HXMS data reveal that five peptides, four of which contain efavirenz contact residues seen in the crystal structure of the RT–EFV complex, show reduced exchange in monomer–EFV complexes. Moreover, peptide 232–246 undergoes slow cooperative unfolding/refolding in the bound monomers, but at a much slower rate than observed in the p66 subunit of RT heterodimer (Seckler, J. M., Howard, K. J., Barkley, M. D., and Wintrode, P. L. (2009) *Biochemistry 48*, 7646–7655). These results suggest that the efavirenz binding site on p66 and p51 monomers is similar to the NNRTI binding pocket in the p66 subunit of RT. Nanoelectrospray ionization FT-ICR mass spectra indicate that the intact monomers each have (at least) two different conformations. In the presence of efavirenz, the mass spectra change significantly and suggest that p51 adopts a single, more compact conformation, whereas p66 undergoes facile, electrospray-induced cleavage. The population shift is consistent with a selected-fit binding mechanism.

HIV-1 reverse transcriptase1 was the first drug target in the treatment of AIDS. Both nucleoside and nonnucleoside reverse transcriptase inhibitors are an essential component of highly active antiretroviral therapy (HAART). Efavirenz and other NNRTIs are a class of small amphiphilic compounds that bind to RT and inhibit viral replication. The biologically active form of RT is an asymmetric heterodimer composed of 66 and 51 kDa subunits (1).

†This work was supported by NIH Grant GM071267.

*To whom correspondence should be addressed. M.D.B.: Phone, 216-368-0602. Fax, 216-368-0604, mdb4@case.edu. P.L.W.: Phone, 216-368-3178. Fax, 216-368-3952., patrick.wintrode@case.edu.

SUPPORTING INFORMATION AVAILABLE
Peptides used for analysis of H/D exchange data (Table S1). This material is available free of charge via the Internet at http://pubs.acs.org.

[1]Abbreviations: CD, circular dichroism; DMF, *N*,*N*-dimethylformamide; EDTA, ethylenediaminetetraacetic acid; EFV, efavirenz; FT-ICR MS, Fourier transform ion cyclotron mass spectrometry; HIV-1, human immunodeficiency virus type 1; HXMS, hydrogen/deuterium exchange mass spectrometry; *m*/*z*, mass-to-charge ratio; nano-ESI, nanoelectrospray ionization; NNRTI, nonnucleoside reverse transcriptase inhibitor; NRTI, nucleoside reverse transcriptase inhibitor; P/T, primer/template; RT, reverse transcriptase; SAXS, small-angle X-ray scattering; Tris, tris(hydroxymethyl)aminomethane

The p66 subunit contains polymerase and RNase H domains (Figure 1). The polymerase domain has four subdomains: fingers (residues 1–85, 118–155), palm (residues 86–117, 156–236), thumb (residues 237–318) and connection (residues 319–426) (2). The p51 subunit comprises the polymerase domain of p66 with a different tertiary fold of the four subdomains. Both the DNA polymerase and RNase H active sites are in the p66 subunit (3). In virus infected cells, the p66 subunit is expressed as part of the 160 kDa Gag-Pol polyprotein, which is subsequently processed by the encoded HIV-1 protease (4). The mechanism of maturation of RT heterodimer is not fully understood. Two models have been proposed (5). In the concerted model, p66 and p51 monomers derived from separate Gag-Pol precursors associate directly to form p66/p51 heterodimer. In the sequential model, two p66 monomers derived from Gag-Pol precursors associate to form a homodimer intermediate. HIV-1 protease then cleaves the C-terminal RNase H domain from one subunit of p66/p66 homodimer to yield mature heterodimer. The sequential mechanism readily explains the 1:1 ratio of p66 and p51 observed in mature virus (6). Processing of 90 kDa Pol polyprotein constructs in bacteria appears to follow a sequential pathway (5). Dimerization of RT is quite slow in solution , suggesting that tmonomeric forms of RT may persist for some time during maturation (7,8).

In solution, RT is a reversible equilibrium mixture of two monomers, two homodimers, and heterodimer; p66/p51 heterodimer is 14-fold more stable than p66/p66 homodimer and 740-fold more stable than p51/p51 homodimer (9). All dimers have enzymatic activity. Efavirenz enhances dimerization of both homo- and heterodimers and processing of polyprotein precursors (9–12). The monomers have folded conformations, but lack activity and do not bind nucleic acid substrates (13). However, recent equilibrium dialysis experiments showed that the two monomers, p66 and p51, bind efavirenz with the same micromolar affinity (14). The binding stoichiometry is one efavirenz per monomer and one efavirenz per homodimer. These results confirmed a thermodynamic linkage between NNRTI binding and subunit dimerization (9). Kinetics experiments using tryptophan fluorescence also showed that efavirenz is a slow binding inhibitor (14). The kinetics data indicate a one-step direct binding mechanism with binding rate constant $k_a = 13.5\ M^{-1}\ s^{-1}$ for p66 and p51 monomers as well as for RT heterodimer. We attributed the slow binding kinetics to conformational selection, where efavirenz preferentially binds to a conformer present at low concentration (15). Additional support for this hypothesis comes from surface plasmon resonance studies indicating that NNRTIs bind to RT by a two-step mechanism consisting of a conformational equilibrium followed by complex formation (16).

Crystal structures of RT with and without bound NNRTIs have identified amino acid contacts and conformational changes associated with inhibitor binding (17). Unfortunately, no structures are available for either monomers or homodimers in the presence or absence of NNRTIs. The NNRTI binding pocket, present only in structures of RT–NNRTI complexes, resides in the palm of the p66 subunit with an additional contact in the p66 thumb and in the p51 fingers. NNRTIs bind ~10 Å away from the polymerase active site and have diverse effects on RT subunit dimerization and enzymatic activities (12,18–20). In the structure of unliganded RT (Figure 1), the amino acid residues in the consensus NNRTI binding pocket are clustered in the two subunits. In the p66 subunit, the efavirenz contact residues are located between the fingers and thumb with side chains pointing inward. In the p51 subunit, these contact residues are located between the palm and thumb with more randomly oriented side chains. The p51 subunit does not form a functional NNRTI binding pocket, as evident from the crystal structures of RT–NNRTI complexes and the binding stoichiometry of the homodimers (14,17).

The equilibrium and kinetics studies of efavirenz binding to monomers raise intriguing questions about the binding site in the monomers. First, is the structure of the bound

monomer different from unbound monomer? If so, this population shift is consistent with the proposed selected-fit binding mechanism (14,16). Second, do p66 and p51 monomers undergo similar conformational changes? The K_ds for p66– and p51–EFV complexes are 2.7 and 2.5 mu;M, suggesting similar binding sites in p66 and p51 (14). Third, do the monomers use the same residues as the heterodimer to bind efavirenz? In the RT–EFV complex, efavirenz makes contacts with L100, K101, K103, V106, V179, Y181, Y188, G190, F227, W229, L234, H235, and P236 in the palm and Y318 in the thumb of the p66 subunit (21–23).

Here we use hydrogen/deuterium exchange mass spectrometry to examine the solution conformation and dynamics of p66 and p51 monomers in the presence of efavirenz. Analysis of the exchange kinetics of protein backbone amide protons provides information on amide hydrogen bonding, flexibility, and local solvent accessibility (24). Amide hydrogens that are located in elements of stable secondary structure, α-helices and β-sheets, exchange slowly compared to amide hydrogens in flexible regions and surface-exposed loops. Comparison of H/D exchange of the two monomers with and without efavirenz reveals how inhibitor binding alters local flexibility and solvent exposure. Additionally, Fourier transform ion cyclotron resonance mass spectrometry is used to examine intact unbound and efavirenz bound monomers.

EXPERIMENTAL PROCEDURES

Materials

Efavirenz was obtained from the NIH AIDS Research and Reference Reagent Program (Germantown, MD). D_2O was purchased from Cambridge Isotope Laboratories (Andover, MA). DMF (DNase, RNase, protease free) was purchased from Acros Organics (Belgium). Biochemical reagents and chemicals were purchased from Roche Applied Science (Indianapolis, IN) and Sigma-Aldrich (St. Louis, MO) unless otherwise specified. RT buffer D is 0.05 M Tris (pH 6.5; RNase, DNase free), 25 mM NaCl, 1 mM EDTA, and 10% (v/v) glycerol (molecular biology grade redistilled). Purification of $p66^{W401A}$ and $p51^{W401A}$ with N-terminal hexahistidine extensions was performed as described (14).

Protein concentrations were determined by absorbance at 280 nm, using ε(280) = 131,780 M^{-1} cm^{-1} for $p66^{W401A}$ and ε (280) = 118,830 M^{-1} cm^{-1} for $p51^{W401A}$ calculated from amino acid sequence (25). Efavirenz (20–250 mM in DMF) was added to protein samples in small increments and the solution was mixed for 2–5 min between additions to avoid protein aggregation. The final concentration of DMF was 0.5% (v/v). As a control, 0.5% (v/v) DMF was also added to protein samples without efavirenz.

CD spectra were recorded on a Jasco J-715 spectropolarimeter as described (26).

Peptide Mapping by Tandem Mass Spectrometry

Peptide mapping experiments were carried out as described (27). Sequencing by tandem mass spectrometry was carried out using a Finnigan™ LTQ quadrupole ion trap mass spectrometer (ThermoElectron). Additional experiments were conducted on an LTQ-FT-ICR mass spectrometer (ThermoElectron) to confirm peptide identification by exact mass.

HXMS

The $p66^{W401A}$ and $p51^{W401A}$ proteins (7.0 mu;g; 20 mu;M) in RT buffer D-H_2O were diluted 10-fold into RT buffer D-D_2O (pD 7.2) containing 5% glycerol and were incubated for various times at 5 ºC. For experiments in the presence of efavirenz, protein samples were incubated with 40 mu;M efavirenz for 15 h at 5 ºC prior to dilution into D_2O buffer

containing 25 mu;M efavirenz. Exchange was quenched by 5-fold dilution into 100 mM NaH_2PO_4 (pH 2.4) at 5 ºC.

The deuterium-labeled protein was digested on ice with 5 mu;L of 1 mg/mL porcine pepsin in H_2O for 5 min and analyzed by HPLC-MS as described elsewhere (28). Deuterium levels for each peptide were corrected for back-exchange using

$$D = \frac{m - m0}{m100 - m0} \times N \quad (1)$$

where *D* is the number of amide hydrogens exchanged with deuterium, *m* is the centroid mass of the peptide at a given time point, *m*0 is the mass of the undeuterated peptide, *m*100 is the mass of the fully deuterated peptide, and *N* is the number of amide hydrogens. Centroid masses of peptides were calculated using MagTran (29). For peptides with double isotopic envelopes, the centroid mass was calculated for the entire range including both low and high *m*/*z* peaks.

FT-ICR MS

Nano-ESI FT-ICR MS was performed on a Bruker Daltonics APEX-QE equipped with a 7 Tesla magnet and Apollo 2 electrospray ionization source. To aid the survival of non-covalent complexes and transmission of higher *m/z* ions, the instrument has been modified to provide an increased pressure (4.7 mbar) in the first vacuum stage by throttling the 1st stage mechanical pump (30). Experimental parameters were carefully tuned to ensure gentle conditions in the ion source, ion guiding, and ion storage regions. With this simple instrumental modification and experimental parameters used, complexes of proteins with sugar molecules (similar in size to efavirenz, which has a molecular weight of 341 Da) are readily observed. Hemoglobin tetramer (64.5 kDa) was used for instrument tuning and calibration. The $p66^{W401A}$ and $p51^{W401A}$ monomers (20 mu;M) were dialyzed overnight at 5 °C into 100 mM NH_4OAc (pH 7.0) and then incubated in the absence or presence of 40 mu;M efavirenz for 15 h at 5 °C. Passive nano-ESI was accomplished using borosilicate tips pulled to a ~3 mu;m opening using a Sutter P-97 capillary puller. A platinum wire inserted into the solution-containing nano-ESI tip acted as a grounded electrode while a potential between –0.9 to –2.0 kV was applied to the inlet to the mass spectrometer. Spectra shown correspond to the transformation of 16 k data points digitized at a rate of 555.6 kHz.

RESULTS

Conformational Changes in Monomer–EFV Complexes

The p66 and p51 monomers contain the dimerization defective W401A substitution to ensure that p66 and p51 remain monomeric in the presence of efavirenz (14,31,32). HXMS was used as described (33). In short, HXMS was monitored at various times after dilution into deuterated buffer. The exchange was quenched, the protein was digested with pepsin, and the fragments were analyzed by LC-MS. The peptic fragments provided ~80% sequence coverage for each monomer (see Table S1). Comparison of CD spectra and HXMS data for wild-type and W401A monomers confirmed that the mutation has no effect on the solution structure (not shown).

Figures 2 and 3 show the full peptide maps of p66 and p51 in the absence and presence of efavirenz. In unbound monomers, most of the peptides show little exchange at 10 s, indicative of secondary structure or inaccessibility to solvent. The exceptions are peptides 210–231 in the palm, 232–246 in the junction between the palm and thumb, 417–425 in the

connection, and 534–560 in the RNase H domain; these peptides are either solvent-exposed loops or unfolded. In bound monomers, peptides 88–109 and 210–231 in the palm, 232–246 in the palm-thumb junction, 257–282 in the thumb, and 301–328 in the thumb-connection junction, are more rigid. Four of these five peptides contain NNRTI binding pocket residues (17), the exception being peptide 257–282 in the thumb. Two other peptides that contain binding pocket residues, 182–187 and 187–192, show very little exchange in either the absence or presence of efavirenz. Additionally, efavirenz has no effect on exchange in the RNase H domain (Figure 2).

The structural changes in the polymerase domain of the two bound monomers are similar. Figure 4 compares the difference in number of deuteria exchanged in the absence and presence of efavirenz for 5 peptides in p66 and p51 after 10, 100, and 1000 s in D_2O. Efavirenz had little effect on the other 44 peptides in the two monomers. The average differences in number of deuteria exchanged were 0.5 ± 0.4 at 10 s, 0.7 ± 0.6 at 100 s, and 0.9 ± 0.8 at 1000 s. A small decrease in exchange at 10 s and reduction in exchange at later times indicates stabilization of existing structure, whereas a large decrease in exchange at 10 s suggests formation of additional secondary structure or solvent exclusion. Therefore, the structure of peptides 88–109 and 257–282 are more rigid in bound monomers. On the other hand, peptides 210–231 and 301–328 have either increased secondary structure or some residues blocked by the inhibitor. Peptide 232–246 undergoes cooperative unfolding/refolding in the presence of efavirenz as described below.

Reversible Cooperative Unfolding/Refolding in Efavirenz Binding Site

HXMS provides the ability to distinguish two types of hydrogen exchange kinetics, correlated exchange EX1 and uncorrelated exchange EX2 (34). EX1 kinetics results in a double isotopic envelope in the mass spectra. The two peaks with low and high *m/z* correspond to two states of the peptide, folded and unfolded. EX1 exchange kinetics is emblematic of slow reversible cooperative unfolding/refolding, which appears irreversible in the presence of excess D_2O. The commonly observed EX2 kinetics shows a gradual shift of a single peak to higher average *m/z*. Figure 5 shows that the exchange kinetics of peptide 232–246 switch from EX2 kinetics in the absence of efavirenz to EX1 kinetics in the presence of the inhibitor. The EX1 mechanism is observed in both p66–EFV and p51–EFV complexes. In the absence of efavirenz, about 80% of the amide hydrogens exchange after 10 s in D_2O, indicating that the peptide is largely unfolded (Figure 5, left panel). In the presence of efavirenz, two populations are clearly present at low and high *m/z* (Figure 5, right panel). For the concentrations used in the HXMS experiments, ~90% of the monomer is bound to efavirenz at equilibrium before and after dilution into D_2O (14). Moreover, the $t_{1/2}$ for unbinding of efavirenz is ~2.1 h (14). The fact that the unfolded peak accounts for ~30% of the total population after only 5 s of incubation in D_2O is therefore unlikely to be an artifact due to unbound monomer. Apparently this local unfolding does not necessarily release the bound efavirenz. The low and high *m/z* peaks were fit to Gaussian distributions. The folded conformation is the major solution structure of peptide 232–246 in the bound monomers. Five and 10 s incubations in D_2O produce little change in the ratio of folded to unfolded peptide. The relative heights of the low and high *m/z* peaks remain approximately constant between 50 and 5000 s. By 2 h almost 50% of the peptide is still protected from exchange. After 4 h, most of the peptide has undergone cooperative unfolding, as evident from the shift to the high *m/z* peak. A very slow rate of cooperative unfolding has also been reported for SH3–HIV Nef peptide complex (35).

Over the course of several hours incubation in D_2O, peptide 232–246 undergoes a mix of both EX1 and EX2 kinetics, as has been observed before in other proteins (34). EX2 exchange is evident as a slight upward mass shift of the low *m/z* peak from ~921 to ~922 *m/z*, corresponding to the exchange of approximately 2 hydrogens with deuterium in the

doubly charged ion. This indicates that the folded state of these residues is not hyperstable, but undergoes the conformational fluctuations typical of folded proteins. The difference in centroid mass of the low and high *m/z* peaks corresponds to exchange of 4 amide hydrogens. In the crystal structures of RT and RT–EFV complex (21,22,36), this peptide comprises β-strands 13 and 14 and a loop in the p66 subunit and is partially unstructured in the p51 subunit. There are 6 amino acids in β-strands 13 and 14, and the 13–14 β-hairpin contains 4 amide hydrogen bonds. The slow unfolding/refolding observed in the presence of efavirenz can therefore be well explained by the cooperative breaking of this hairpin. Additionally, the preceding peptide 210–231 exchanges 8 fewer amide hydrogens in bound than in unbound monomers (Figure 4). In the structure of RT-EFV complex this peptide has 9 amino acids forming secondary structures. The decrease in exchange in peptides 210–231 and 232–246 in bound monomers is consistent with formation of structural elements similar to those of the p66 subunit in the RT–EFV complex.

Multiple Populations of Unbound Monomers

Transferring intact proteins and their complexes from solution to the gas phase is possible using electrospray ionization (37,38). The charge-state distribution of electrosprayed protein ions reflects the compactness of the protein in solution. Generally, unfolded proteins exhibit a relatively broad distribution centered around higher charge states in ESI mass spectra, whereas the same proteins when folded produce narrower distributions centered around lower charge states (39,40). Nano-ESI was used to produce intact multiply charged ions of p66 and p51 in the absence and presence of efavirenz. Figure 6a,c presents the mass spectra of p51 and p66 obtained in the absence of efavirenz. The spectra of the monomers each show two distinct charge-state envelopes. For p51 monomer, a distribution centered around the 15+ charge state is the most intense, while there is a second distribution centered around the 20+ charge state. For p66 monomer, the main distribution is centered around the 18+ charge state, while a smaller distribution centered around the 22+ charge state is also apparent. The presence of two charge-state envelopes in each spectrum indicates the existence of at least two different solution conformations of both monomers. The lower charge-state distributions, present at higher *m/z*, most likely correspond to relatively more folded structures of each monomer. Unfortunately, there is not a straightforward quantitative relationship between relative charge-state peak intensities in ESI mass spectra and solution populations of proteins. Several factors may lead to discrimination against higher charge states during ESI (41), and ion transmission efficiencies within the mass spectrometer depend on *m/z* and instrumental conditions. Therefore the relative intensities of the 2 distributions may not reflect the relative solution populations.

The calculated mass of p51 (52,797 Da) is in good agreement with the measured mass (52,790 ± 10 Da) (Figure 6a). The ESI mass spectrum of p66 is complicated by the existence of two major species of masses differing by 340 Da, giving the appearance of splitting peaks (Figure 6c). The measured mass of the species marked with a circle (65,890 ± 10 Da) agrees with the calculated mass of p66 (65,900 Da). A species with a mass lower by 340 Da is also present. This may correspond to either a deletion mutant or degradation product of the protein. DNA sequencing of the $p66^{W401A}$ gene confirmed the correct sequence (14), making a deletion in the protein unlikely, and peptide mapping did not show missing amino acids in the 80% coverage provided by peptic fragments. Both the facts that peaks in the ESI mass spectrum of the p51 monomer correspond to a single mass, and that upon fragmentation (see below) only a single dominant mass is observed, suggest that the difference between the 65,890 and 65,550 species occurs in the C-terminal RNase H domain of the p66 monomer. However, no tandem mass spectrometry was carried out to identify a degradation product. Additional smaller peaks are observable at *m/z* greater than 3400.

These have the appearance of non-covalent adducts (mass ~320 Da) associated with the more folded (lower charge state) conformation of the protein.

While the p51–EFV complex was not directly detected despite the use of soft ESI conditions (see Experimental Procedures), the effect of the drug on the protein mass spectrum is dramatic. In the presence of efavirenz, the higher charge-state distribution disappears from the ESI mass spectrum of p51 and only the lower charge-state distribution remains (Figure 6b). Moreover, the new charge-state distribution is centered one charge lower than the most intense charge state in the absence of efavirenz. This indicates that binding of efavirenz shifts the equilibrium of two unbound populations to one bound conformational state. Furthermore, the data suggest that the conformation of the p51–EFV complex is relatively compact.

The nano-ESI mass spectra of p66 in the presence of efavirenz also show dramatic changes resulting from binding of the inhibitor. Figure 6d shows the mass spectrum recorded immediately after applying the nano-ESI voltage to the tip, while panel Figure 6e shows a mass spectrum recorded after 3 min of nano-ESI. No peak corresponding to p66–EFV complex was observed. Instead, peaks corresponding to p66 rapidly decrease in intensity, while signal corresponding to a 47 kDa species grows in with time. This behavior is highly unusual and markedly different from that observed for p66 without efavirenz and for p51 with or without inhibitor, all of which showed nano-ESI mass spectra that did not change appreciably with time. Adjustment and optimization of the instrument to ensure very gentle source conditions did not prevent the fragmentation. The rapid disappearance of p66 and appearance of the 47 kDa species upon application of ESI voltage was reproducible, occurring with multiple samples in different nano-ESI tips on multiple days. With each new ESI tip, the p66 was clearly visible for a short time prior to its disappearance. Thus, the truncation of p66 is induced by the nano-ESI, implying that efavirenz binding renders p66 more susceptible to cleavage during ESI. Although infrequent, electrospray-induced reactions have been observed previously; the most common of these is oxidation (42, 43). The 47 kDa fragment may correspond to cleavage after residue 393, either to form a b-type ion or a c-type ion (calculated masses 46,996 and 47,013 Da, respectively, compared to 47,010 Da measured mass). The same species is present in extremely low abundance in the mass spectrum of p66 in the absence of efavirenz (Figure 6c) and in the mass spectrum of p51 in the presence of efavirenz (Figure 6b). The mass spectra shown in Figure 6d,e further suggest that a fraction of the proteins unfold prior to cleavage (distribution centered around 25+ charge state) and that the more compactly folded proteins (centered around the 16+ charge state) are cleaved more slowly.

At first glance, results from H/D exchange and ESI charge-state distributions may seem inconsistent. Peptide 232–246 shows a single population in the absence of efavirenz and 2 populations when efavirenz is bound. In contrast, ESI of the intact monomers shows at least 2 populations in the absence of efavirenz and a single population when bound. This apparent contradiction can be understood by appreciating the meaning of the areas under the 2 peaks that arise from EX1 exchange. When the rate of refolding in a reversible unfolding/refolding reaction is slower than the intrinsic rate of H/D exchange (a requirement for EX1 exchange) the area under the peak corresponding to the unfolded form does not represent the instantaneous population of the unfolded state. Rather, it reflects the fraction of the population that has visited the unfolded state at least once during the time of incubation in D_2O. In the case of peptide 232–246 in the presence of efavirenz, while this region clearly samples the unfolded state, the fraction of the total RT in solution occupying the unfolded state at any given time may be quite small, and thus consistent with the lack of a detectable higher charge-state distribution in ESI. In any case, both H/D exchange and ESI of intact

monomers indicate that efavirenz binding stabilizes a distribution of more tightly folded conformations.

DISCUSSION

Efavirenz is an NNRTI capable of affecting several steps in HIV-1 reverse transcription and replication (12,19,44). Analysis of dose-response curves for anti-HIV-1 drugs shows that the slope values are class specific (45). NNRTIs, protease, and fusion inhibitors have slopes >1, whereas NRTIs and integrase inhibitors have slopes ~1 typical of noncooperative processes. Drugs with slopes >1 are more potent inhibitors in single-round infectivity assays, presumably because they target multiple copies of the proteins themselves. In the case of reverse transcriptase, NRTIs target a single RT–P/T complex undergoing nucleotide addition and chain termination. NNRTIs, on the other hand, inhibit DNA polymerization, perturb RNase H activity, and enhance dimerization. We have recently shown that efavirenz also binds p66 and p51 monomers, a completely new function of NNRTIs for which the biological significance is as yet unknown (14). However, p66 monomer is presumably present at some point in the life cycle of the virus and thus a potential target for drug design. Although equilibrium and kinetics studies defined the binding constants and binding mechanism for p66– and p51–EFV complexes, the binding site on the monomers is not known. We used HXMS along with FT-ICR MS to begin elucidating the monomer binding sites and the conformational selection process of NNRTI binding in both monomers and heterodimer.

The HXMS results show that efavirenz binding rigidifies the same 5 peptides in the polymerase domains of p66 and p51. The two subunits of RT have different configurations in the crystal structure of the heterodimer. The polymerase domain of the p66 subunit has an “open” conformation that contains the polymerase active site; the p51 subunit has a “closed” conformation that conceals the active site residues site (46). In almost all NNRTI–RT complexes, the p66 polymerase domain has an “extended” open conformation (47). In the absence of structures for the monomers, the 5 peptides that become more folded in the presence of efavirenz are mapped onto separate views of the p66 and p51 subunits from the crystal structure of the RT–EFV complex (Figure 7). While identical peptides are affected in the two monomers, the secondary and tertiary structures of these peptides are quite different in the two subunits of the heterodimer. In the p66 subunit structure, the 5 affected peptides are contiguous and concentrated in the vicinity of the NNRTI binding pocket; 4 of these peptides contain NNRTI binding pocket residues. Exact localization of the efavirenz binding site in the monomers is complicated by the peptide-level resolution of HXMS. Moreover, the relatively large portion of each monomer (120 residues) whose H/D exchange is altered by binding clearly indicates that efavirenz has allosteric effects on molecular flexibility, particularly in peptides 257–282 and 301–28. Nevertheless, the profound stabilization of β-strands 13 and 14, together with the fact that 4 of 5 peptides affected by binding contain at least 1 drug contact residue, strongly suggests that the efavirenz binding site is quite similar in RT monomers and heterodimer. Furthermore, HXMS shows that these same 5 peptides are also rigidified in RT heterodimer in the presence of efavirenz (48). These results argue that the conformation of the polymerase domain of bound monomers is similar to that of the p66 subunit in RT. This is supported by the fact that both homodimers have polymerase activity (7,49), in which one subunit must have a catalytically active “open” conformation similar to the p66 subunit of the heterodimer. NMR studies monitoring [*methyl*-^{13}C]methionine residues confirm that both p51/p51 homodimer and p66/p51 heterodimer have asymmetric structures in solution (50,51). SAXS data for p51 suggest that one subunit of the homodimer adopts the closed conformation, while the other subunit is in either the open or extended conformation in the absence or presence of the NNRTI

nevirapine (50). The polymerase domain of both p66 and p51 appears capable of adopting at least 3 conformations: open, closed, and extended.

Previous HXMS studies of RT found that peptide 232–246, located at the base of the thumb, undergoes EX1 exchange due to slow cooperative unfolding of β-strands 13 and 14 with $t_{1/2}$ ~20 s (33). No evidence for EX1 exchange or two conformationally distinct populations of this peptide is seen in the unbound monomers. In the presence of efavirenz, there are clearly 2 slowly interconverting populations. However, the interconversion rate is markedly slower than that of unliganded RT, although comparable to the interconversion rate of RT-EFV complex (48). The enhanced local folding is accompanied by stabilization of the structure of the other 4 peptides in the palm and thumb. Examination of the amino acid sequence of these peptides shows multiple Lys, Arg, and His residues: 5 in peptides 88–109 and 210–231, 2 in peptide 232–246, and 4 in peptides 257–282 and 299–328. Stabilization of the peptides may sequester these side chains as well as amide nitrogens or carbonyl oxygens, thereby changing the exposed surface area and reducing the ability to gain a charge during ESI. This is consistent with the shift in the ESI charge-state distributions to a more folded conformation with lower charge state in the presence of efavirenz. The fact that both low and high charge-state distributions are clearly evident in the absence of efavirenz suggests a conformational selection/population shift mechanism of binding-associated conformational change. In such a mechanism, the “compact” efavirenz binding-competent state is present in the absence of efavirenz, and efavirenz binding stabilizes this conformation and shifts the rest of the population out of the less compact binding-incompetent conformations. If the binding-competent form represents a minority population in solution in the absence of efavirenz, this conformational selection might help explain the slow binding of efavirenz (14).

Supplementary Material

Refer to Web version on PubMed Central for supplementary material.

Acknowledgments

We are grateful to James M. Seckler for helpful discussions of HXMS data and to Matthew Forbes for technical help in FT-ICR MS experiments.

References

1. Wang J, Smerdon SJ, Jäger J, Kohlstaedt LA, Rice PA, Friedman JM, Steitz TA. Structural basis of asymmetry in the human immunodeficiency virus type 1 reverse transcriptase heterodimer. Proc Natl Acad Sci USA. 1994; 91:7242–7246. [PubMed: 7518928]
2. Kohlstaedt LA, Wang J, Friedman JM, Rice PA, Steitz TA. Crystal structure at 3.5 Å resolution of HIV-1 reverse transcriptase complexed with an inhibitor. Science. 1992; 256:1783–1790. [PubMed: 1377403]
3. Le Grice SFJ, Naas T, Wohlgensinger B, Schatz O. Subunit-selective mutagenesis indicates minimal polymerase activity in heterodimer-associated p51 HIV-1 reverse transcriptase. Embo J. 1991; 10:3905–3911. [PubMed: 1718745]
4. Coffin, JM.; Hughes, SH.; Varmus, HE. Retroviruses. Cold Spring Harbor Laboratory Press; Woodbury, NY: 1997.
5. Sluis-Cremer N, Arion D, Abram ME, Parniak MA. Proteolytic processing of an HIV-1 pol polyprotein precursor: insights into the mechanism of reverse transcriptase p66/p51 heterodimer formation. Int J Biochem Cell Biol. 2004; 36:1836–1847. [PubMed: 15183348]
6. di Marzo Veronese F, Copeland TL, DeVico AL, Rahman R, Oroslan S, Gallo RC, Sarngadharan MG. Characterization of highly immunogenic p66/p51 as reverse transcriptase of HTLV-III/LAV. Science. 1986; 231:1289–1291. [PubMed: 2418504]

7. Restle T, Müller B, Goody RS. Dimerization of human immunodeficiency virus type 1 reverse transcriptase. J Biol Chem. 1990; 265:8986–8988. [PubMed: 1693146]
8. Venezia CF, Meany BJ, Braz VA, Barkley MD. Kinetics of association and dissociation of HIV-1reverse transcriptase subunits. Biochemistry. 2009; 48:9084–9093. [PubMed: 19715314]
9. Venezia C, Howard KJ, Ignatov ME, Holladay LA, Barkley MD. Effects of efavirenz binding on the subunit equilibria of HIV-1 reverse transcriptase. Biochemistry. 2006; 45:2779–2789. [PubMed: 16503633]
10. Tachedjian G, Moore KL, Goff SP, Sluis-Cremer N. Efavirenz enhances the proteolytic processing of an HIV-1 pol polyprotein precursor and reverse transcriptase homodimer formation. FEBS Letters. 2005; 579:379–384. [PubMed: 15642347]
11. Tachedjian G, Orlova M, Sarafianos SG, Arnold E, Goff SP. Nonnucleoside reverse transcriptase inhibitors are chemical enhancers of dimerization of the HIV type 1 reverse transcriptase. Proc Natl Acad Sci USA. 2001; 98:7188–7193. [PubMed: 11416202]
12. Figueiredo A, Moore KL, Mak J, Sluis-Cremer N, de Bethune MP, Tachedjian G. Potent nonnucleoside reverse transcriptase inhibitors target HIV-1 Gag-Pol. PLoS Pathogens. 2006; 2:1051–1059.
13. Ignatov ME, Berdis AJ, Le Grice SFJ, Barkley MD. Attenuation of DNA replication by HIV-1 reverse transcriptase near the central termination sequence. Biochemistry. 2005; 44:5346–5356. [PubMed: 15807528]
14. Braz VA, Holladay LA, Barkley MD. Efavirenz binding to HIV-1 reverse transcriptase monomers and dimers. Biochemistry. 2010; 49:601–610. [PubMed: 20039714]
15. Weikl TR, von Deuster C. Selected-fit versus induced-fit protein binding: kinetic differences and mutational analysis. Proteins: Struct, Funct, Bioinf. 2009; 75:104–110.
16. Geitmann M, Unge T, Danielson UH. Biosensor-based kinetic characterization of the interaction between HIV-1 reverse transcriptase and non-nucleoside inhibitors. J Med Chem. 2006; 49:2367–2374. [PubMed: 16610780]
17. Das K, Lewi PJ, Hughes SH, Arnold E. Crystallography and the design of anti-AIDS drugs: conformational flexibility and positional adaptability are important in the design of non-nucleoside HIV-1 reverse transcriptase inhibitors. Prog Biophys Mol Biol. 2005; 88:209–231. [PubMed: 15572156]
18. Sluis-Cremer N, Dmitrienko GI, Balzarini J, Camarasa MJ, Parniak MA. Human immunodeficiency virus type I reverse transcriptase dimer destablilization by 1-{spiro[4”-amino-2”,2”-dioxo-1”,2”-oxathiole-5”,3’-[2’,5’-bis-*O*-(*tert*-butyldimethylsilyl)-β-D-ribofuranosyl]]}-3-ethylthymine. Biochemistry. 2000; 39:1427–1433. [PubMed: 10684624]
19. Sluis-Cremer N, Tachedjian G. Mechanisms of inhibition of HIV replication by non-nucleoside reverse transcriptase inhibitors. Virus Res. 2008; 134:147–156. [PubMed: 18372072]
20. Spence RA, Kati WM, Anderson KS, Johnson KA. Mechanism of inhibition of HIV-1 reverse transcriptase by nonnucleoside inhibitors. Science. 1995; 267:988–993. [PubMed: 7532321]
21. Lindberg J, Sigurdsson S, Löwgren S, Andersson HO, Sahlberg C, Noréen R, Fridborg K, Zhang H, Unge T. Structural basis for the inhibitory efficacy of efavirenz (DMP-266), MSC194 and PNU142721 towards the HIV-1 RT K103N mutant. Eur J Biochem. 2002; 269:1670–1677. [PubMed: 11895437]
22. Ren J, Milton J, Weaver KL, Short SA, Stuart DI, Stammers DK. Structural basis for the resilience of efavirenz (DMP-266) to drug resistance mutations in HIV-1 reverse transcriptase. Structure. 2000; 8:1089–1094. [PubMed: 11080630]
23. Sobolev V, Sorokine A, Prilusky J, Abola EE, Edelman M. Automated analysis of interatomic contacts in proteins. Bioinformatics. 1999; 15:327–332. [PubMed: 10320401]
24. Wales TE, Engen JR. Hydrogen exchange mass spectrometry for the analysis of protein dynamics. Mass Spectrom Rev. 2006; 25:158–170. [PubMed: 16208684]
25. Leavitt S, Freire E. Direct measurement of protien binding energetics by isothermal titration calorimetry. Curr Opin Struct Biol. 2001; 11:560–566. [PubMed: 11785756]
26. Tachedjian G, Radzio J, Sluis-Cremer N. Relationship between enzymatic activity and dimeric structure of recombinant HIV-1 reverse transcriptase. Proteins: Struct, Funct, Bioinf. 2005; 60:5–13.

27. Tsutsui Y, Liu L, Gershenson A, Wintrode PL. The conformational dynamics of a metastable serpin studied by hydrogen exchange and mass spectrometry. Biochemistry. 2006; 45:6561–6569. [PubMed: 16716066]
28. Zhang Z, Smith DL. Determination of amide hydrogen exchange by mass spectrometry: a new tool for protein structure elucidation. Protein Sci. 1993; 2:779–791.
29. Zhang, Z. MagTran. (the magic transformer), http://www.geocities.com/SiliconValley/Hills/2679/magtran.html
30. Sobott F, Hernández H, McCammon MG, Tito MA, Robinson CV. A tandem mass spectrometer of improved transmission and analysis of large macromolecular assemblies. Anal Chem. 2002; 74:1402–1407. [PubMed: 11922310]
31. Braz VA, Howard KJ. Separation of protein oligomers by blue native gel electrophoresis. Anal Biochem. 2009; 388:170–172. [PubMed: 19233117]
32. Tachedjian G, Aronson HEG, de los Santos M, Seehra J, McCoy JM, Goff SP. Role of residues in the tryptophan repeat motif for HIV-1 reverse transcriptase dimerization. J Mol Biol. 2003; 326:381–396. [PubMed: 12559908]
33. Seckler JM, Howard KJ, Barkley MD, Wintrode PL. Solution structural dynamics of HIV-1 reverse transcriptase heterodimer. Biochemistry. 2009; 48:7646–7655. [PubMed: 19594135]
34. Weis DD, Wales TE, Engen JR, Hotchko M, Ten Eyck LF. Identification and characterization of EX1 kinetics in H/D exchange mass spectrometry by peak width analysis. J Am Soc Mass Spectrom. 2006; 17:1498–1509. [PubMed: 16875839]
35. Engen JR, Smithgall TE, Gmeiner WH, Smith DL. Identification and localization of slow, natural, cooperative unfolding in the hematopoietic cell kinase SH3 domain by amide hydrogen exchange and mass spectrometry. Biochemistry. 1997; 36:14384–14391. [PubMed: 9398156]
36. Hsiou Y, Ding J, Das K, Clark AD Jr, Hughes SH, Arnold E. Structure of unliganded HIV-1 reverse transcriptase at 2.7 Å resolution: implications of conformational changes for polymerization and inhibition mechanisms. Structure. 1996; 4:853–857. [PubMed: 8805568]
37. Benesch JLP, Ruotolo BT, Simmons DA, Robinson CV. Protein complexes in the gas phase: technology for structural genomics and proteomics. Chem Rev. 2007; 107:3544–3567. [PubMed: 17649985]
38. Fenn JB, Mann M, Meng CK, Wong SF, Whitehouse CM. Electrospray ionization for mass spectrometry of large biomolecules. Science. 1989; 246:64–71. [PubMed: 2675315]
39. Chowdhury SK, Katta V, Chait BT. Probing conformational changes in proteins by mass spectrometry. J Am Chem Soc. 1990; 112:9012–9013.
40. Konermann L, Douglas DJ. Acid-induced unfolding of cytochrome *c* at different methanol concentrations: electrospray ionization mass spectrometry specifically monitors changes in tertiary structure. Biochemistry. 1997; 36:12296–12302. [PubMed: 9315869]
41. Kaltashov, IA.; Eyles, SJ. Mass Spectrometry in Biophysics. John Wiley & Sons; Hoboken, NJ: 2005.
42. Chen ML, Cook KD. Oxidation artifacts in the electrospray mass spectrometry of Aβ peptide. Anal Chem. 2007; 79:2031–2036. [PubMed: 17249640]
43. Van Berkel GL, Asano KG, Schnier PD. Electrochemical processes in a wire-in-a-capillary bulk-loaded, nano-electrospray emitter. J Am Soc Mass Spectrom. 2001; 12:853–862. [PubMed: 11444609]
44. Grobler JA, Dornadula G, Rice MR, Simcoe AL, Hazuda DJ, Miller MD. HIV-1 reverse transcriptase plus-strand initiation exhibits preferential sensitivity to non-nucleoside reverse transcriptase inhibitors *in vitro*. J Biol Chem. 2007; 282:8005–8010. [PubMed: 17172472]
45. Shen L, Peterson S, Sedaghat AR, McMahon MA, Callender M, Zhang H, Zhou Y, Pitt E, Anderson KS, Acosta EP, Siliciano RF. Dose-response curve slope sets class-specific limits on inhibitory potential of anti-HIV drugs. Nat Med. 2008; 14:762–766. [PubMed: 18552857]
46. Jacobo-Molina A, Ding J, Nanni RG, Clark AD Jr, Lu X, Tantillo C, Williams RL, Kamer G, Ferris AL, Clark P, Hizi A, Hughes SH, Arnold E. Crystal structure of human immunodeficiency virus type 1 reverse transcriptase complexed with double-stranded DNA at 3.0 Å resolution shows bent DNA. Proc Natl Acad Sci USA. 1993; 90:6320–6324. [PubMed: 7687065]

47. Ren J, Stammers DK. Structural basis for drug resistance mechanisms for non-nucleoside inhibitors of HIV reverse transcriptase. Virus Res. 2008; 134:157–170. [PubMed: 18313784]

48. Seckler JM, Barkley MD, Wintrode PL. Allosteric supression of HIV-1 reverse transcriptase structural dynamics upon inhibitor binding. Biophys J. 2010 in press.

49. Bavand MR, Wagner R, Richmond TJ. HIV-1 reverse transcriptase: polymerization properties of the p51 homodimer compared to the p66/p51 heterodimer. Biochemistry. 1993; 32:10543–10552. [PubMed: 7691176]

50. Zheng X, Mueller GA, Cuneo MJ, DeRose EF, London RE. Homodimerization of the p51 subunit of HIV-1 reverse transcriptase. Biochemistry. 2010; 49:2821–2833. [PubMed: 20180596]

51. Zheng X, Mueller GA, DeRose EF, London RE. Solution characterization of [methyl-^{13}C]methionine HIV-1 reverse transcriptase by NMR spectroscopy. Antiviral Res. 2009; 84:205–214. [PubMed: 19665484]

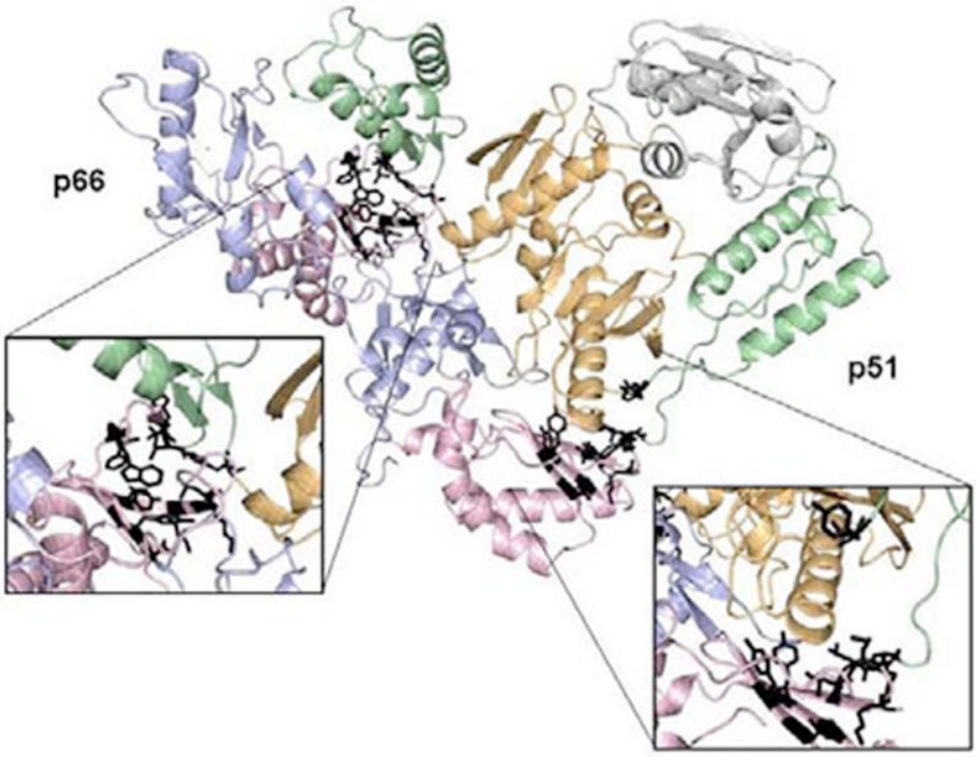

FIGURE 1.
Crystal structure of unliganded HIV-1 RT (1DLO). Four subdomains of the polymerase domain in p66 and p51 subunits: (blue) fingers, (pink) palm, (green) thumb, and (orange) connection; (grey) RNase H domain of p66 subunit; (black) efavirenz contact residues with side chains in p66 and p51 subunits.

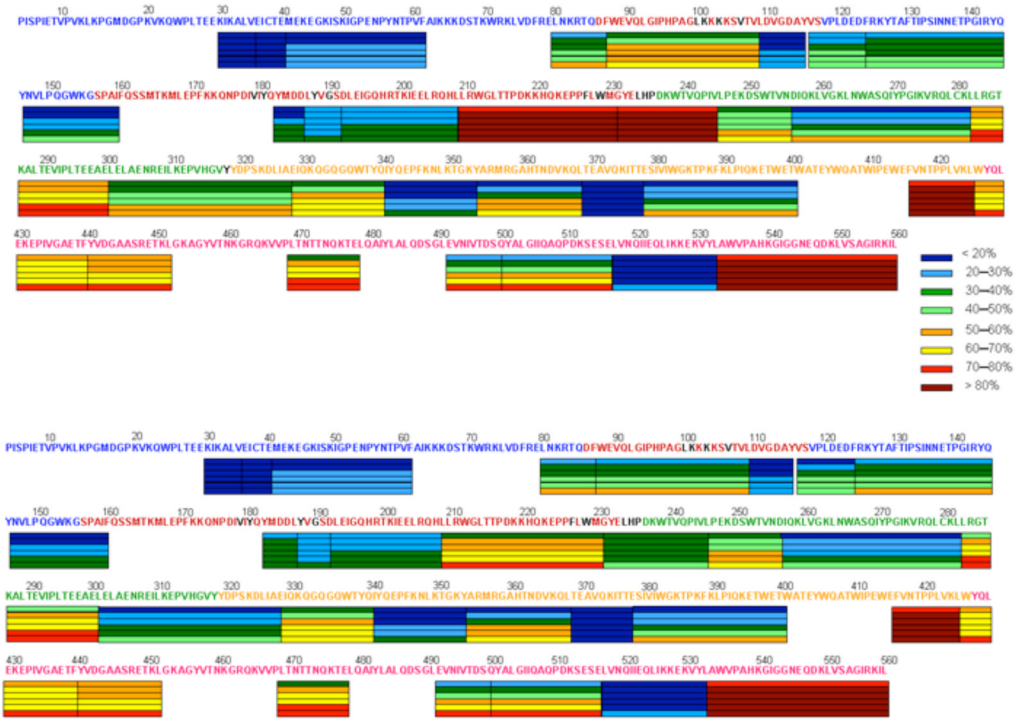

FIGURE 2.

Percent exchange of peptides in p66^{W401A} monomer in (upper) absence and (lower) presence of efavirenz. Color of amino acid sequence indicates subdomains: (blue) fingers, (red) palm, (green) thumb, and (orange) connection; (magenta) RNase H domain; (black) efavirenz contact residues. Colored bars below sequence from top to bottom give exchange at 10, 50, 100, 500, 1000, and 5000 s.

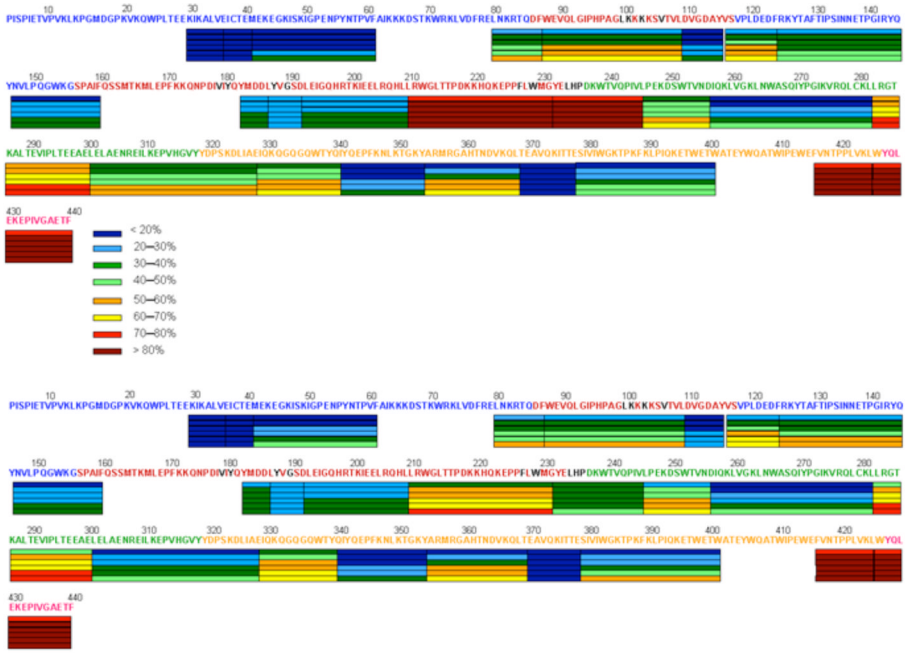

FIGURE 3.

Percent exchange of peptides in p51^{W401A} monomer in (upper) absence and (lower) presence of efavirenz. Color of amino acid sequence indicates subdomains: (blue) fingers, (red) palm, (green) thumb, and (orange) connection; (black) efavirenz contact residues. Colored bars below sequence from top to bottom give exchange at 10, 50, 100, 500, 1000, and 5000 s.

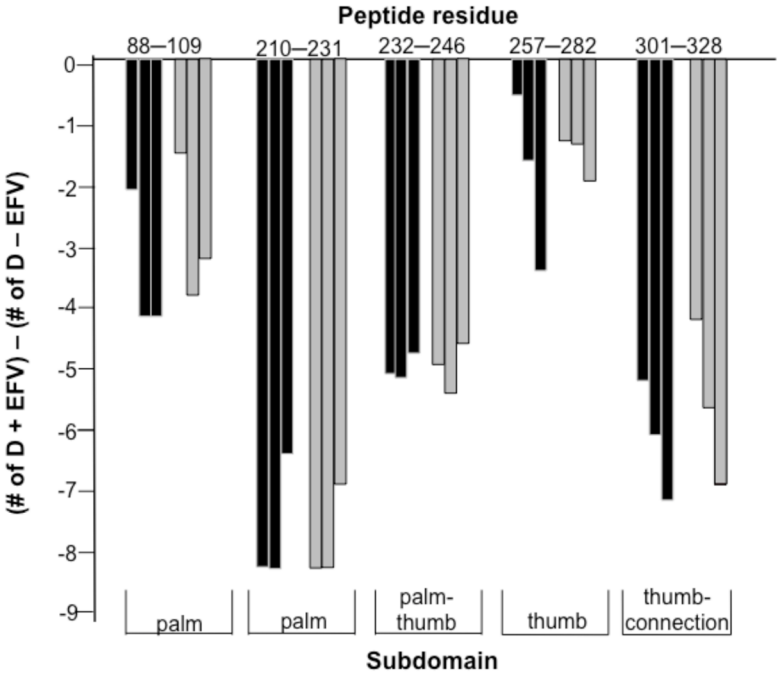

FIGURE 4.

Difference in number of deuteria exchanged in bound and unbound p66 and p51. Difference calculated by subtracting the exchange in unbound monomer from the exchange in the monomer–EFV complex. Differences are shown for (black) $p66^{W401A}$ and (grey) $p51^{W401A}$ after (left) 10 s, (middle) 100 s, and (right) 1000 s.

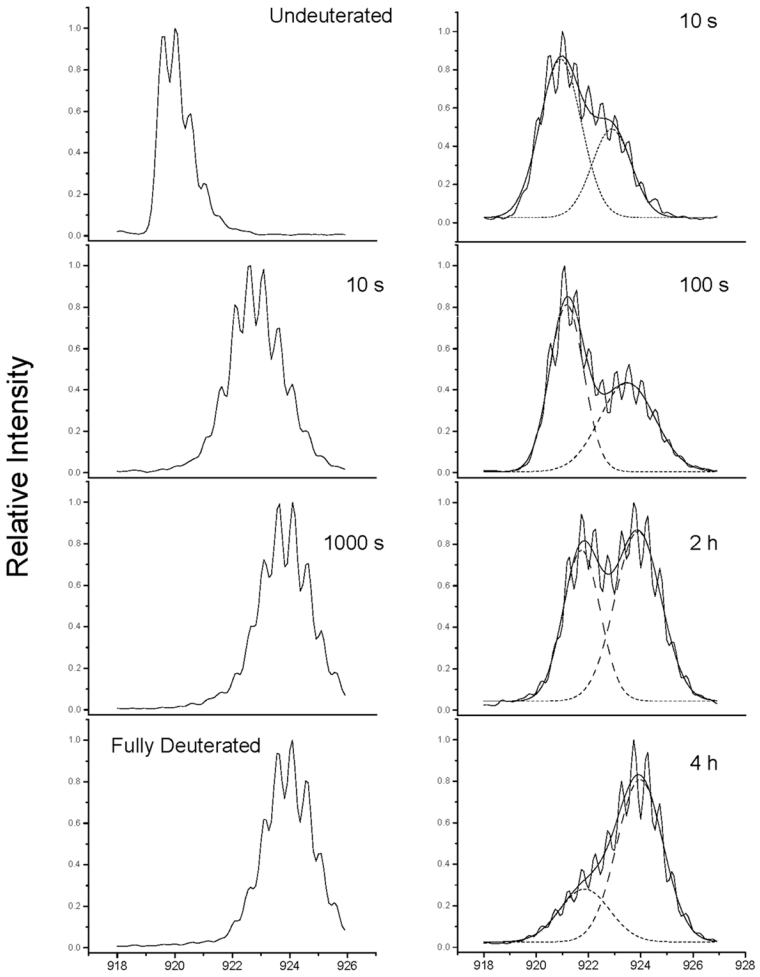

FIGURE 5.

Mass spectra of peptide 232–246 in (left) $p51^{W401A}$ and (right) $p51^{W401A}$–EFV complex after different incubations times in RT buffer D-D_2O. Low and high *m/z* peaks for $p51^{W401A}$–EFV complex fit to Gaussian distributions (dashed lines).

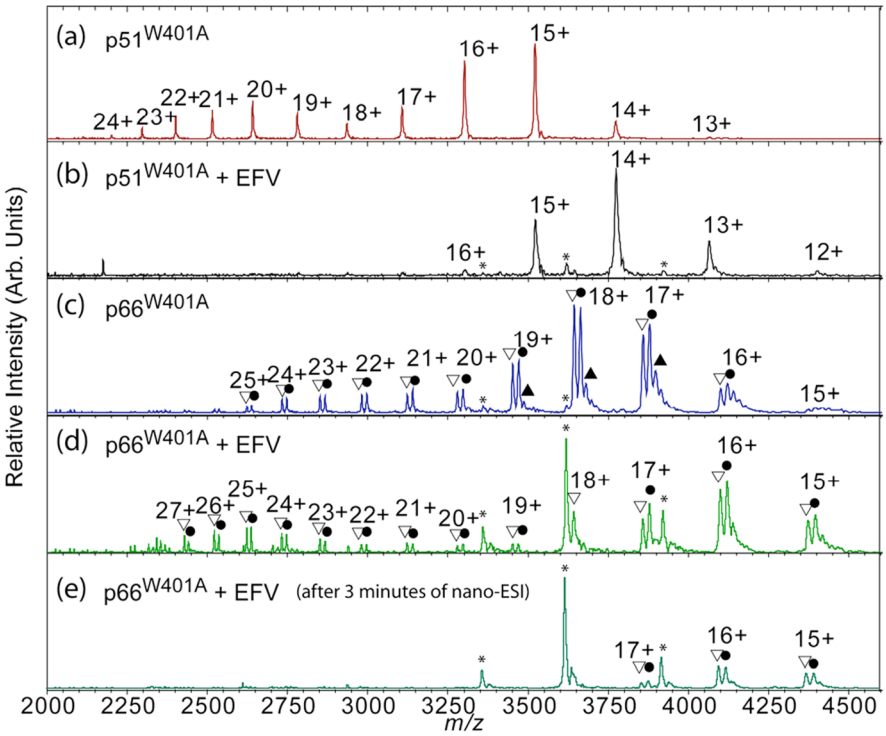

FIGURE 6.

Nano-ESI mass spectra of (a) $p51^{W401A}$, (b) $p51^{W401A}$–EFV complex, (c) $p66^{W401A}$, (d) $p66^{W401A}$–EFV complex upon initiation of nano-ESI, and (e) $p66^{W401A}$–EFV complex after 3 min of nano-ESI. For $p51^{W401A}$ in the absence and presence of EFV, the deconvoluted mass is 52,790 Da. Deconvoluted masses for $p66^{W401A}$ are (▲) 66,210 Da, (●) 65,890 Da, and (▽) 65,550 Da. The peaks marked with (*) correspond to a 47 kDa truncated protein.

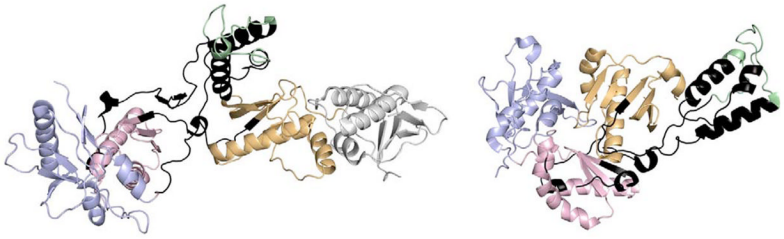

FIGURE 7.

Five peptides stabilized in $p66^{W401A}$– and $p51^{W401A}$–EFV complexes shown in black on the subunits of p66/p51–EFV complex: (left) p66 subunit and (right) p51 subunit from crystal structure of HIV-1 RT–EFV complex (1FK9). Four subdomains of the polymerase domain: (blue) fingers, (pink) palm, (green) thumb, and (orange) connection; (grey) RNase H domain of p66.